The Journal of Chemical Physics ARTICLE pubs.aip.org/aip/jcp

Invariant dynamics in a united-atom model of an ionic liquid

Cite as: J. Chem. Phys. 160, 034503 (2024); doi: 10.1063/5.0177373
Submitted: 21 September 2023 • Accepted: 11 December 2023 •
Published Online: 17 January 2024

Peter A. Knudsen,[1] David M. Heyes,[2] Kristine Niss,[1] Daniele Dini,[2] and Nicholas P. Bailey[1,a)]

AFFILIATIONS

[1] "Glass and Time," IMFUFA, Department of Science and Environment, Roskilde University, P.O. Box 260, DK-4000 Roskilde, Denmark
[2] Department of Mechanical Engineering, Imperial College London, South Kensington Campus, London SW7 2AZ, United Kingdom

[a)] **Author to whom correspondence should be addressed:** nbailey@ruc.dk

ABSTRACT

We study a united-atom model of the ionic liquid 1-butyl-1-methylpyrrolidinium bis(trifluoromethyl)sulfonylamide to determine to what extent there exist curves in the phase diagram along which the microscopic dynamics are invariant when expressed in dimensionless, or reduced, form. The initial identification of these curves, termed isodynes, is made by noting that contours of reduced shear viscosity and reduced self-diffusion coefficient coincide to a good approximation. Choosing specifically the contours of reduced viscosity as nominal isodynes, further simulations were carried out for state points on these, and other aspects of dynamics were investigated to study their degree of invariance. These include the mean-squared displacement, shear-stress autocorrelation function, and various rotational correlation functions. These were invariant to a good approximation, with the main exception being rotations of the anion about its long axis. The dynamical features that are invariant have in common that they are aspects that would be relevant for a coarse-grained description of the system; specifically, removing the most microscopic degrees of freedom in principle leads to a simplification of the potential energy landscape, which allows for the existence of isodynes.

I. INTRODUCTION

The phenomenon of density scaling of dynamics has, in the last two decades, become an important tool for classifying and understanding the behavior of liquids[1–3] (although similar approaches have existed for longer[4]). Density scaling refers to the fact that for many liquids, the dependence of many dynamical quantities on thermodynamic variables can be expressed through a particular combination of density ρ and temperature T, specifically

$$X = f(h(\rho)/T), \tag{1}$$

where X is some dynamical quantity, for example, a relaxation time, $h(\rho)$ is a function that depends on the material, and f is a function that is different for different observables. In many cases, it can be approximated by a power law, $h(\rho) = \rho^{\gamma}$, where the so-called density-scaling exponent γ is a material constant. The essence of density scaling can be stated as the dynamical properties being invariant along certain curves in the phase diagram given by $h(\rho)/T$ = const. The realization of its significance was prompted by the rise of high pressure measurements of glass-forming and other complex liquids. The use of an extra parameter allows for a more complete picture of what governs dynamical behavior. The term density scaling usually refers to the finding that the main relaxation time, τ, and the viscosity can be represented as a function of $h(\rho)/T$.[5,6] In addition to these "scalar" quantities, it is also often found that the spectral shape of the relaxation seen, for example, in dielectric or neutron spectroscopy, is invariant along the lines of constant relaxation time.[1,7–9] This result is called isochronal superposition, but it also leads to a generalization of density scaling[9] (if the relaxation time obeys density scaling) because it follows that any shape parameter of the spectrum will be a function of $h(\rho)/T$. In other words, for some liquids, it is found that the lines in the phase diagram defined by $h(\rho)/T$ = const exhibit identical dynamics as probed by different observables on all time scales.[10,11]

A theoretical concept, hidden scale invariance, and a theoretical framework known as isomorph theory have emerged that can explain density scaling.[12–14] In fact, these lead to a stronger claim, namely that microscopic structure is also invariant on the same

curves as dynamics; these curves are now designated as *isomorphs* to emphasize the invariance of structure. The theory specifies how to quantify the degree to which dynamical invariance can be expected and how to identify isomorphs themselves using methods that are straightforward in computer simulations (at least for the simplest model systems) but less so in experiments. Systems that have good isomorphs are understood to include van der Waals liquids and metals. Typical values of γ for such systems are in the range 4–8 for van der Waals systems (though lower for polymers)[15] and 2–6 for metals.[16] Those systems in which Coulomb interactions dominate or have strong directional bonds, e.g., in the form of hydrogen bonds, as in, for example, water, do not have good isomorphs in simulations.[17,18] In experiments, there is some evidence that density scaling breaks down for hydrogen bonding systems, particularly when it comes to the spectral shape being invariant over many decades in time and/or at very high (GPa-range) pressures.[10,19,20] This breakdown is expected from isomorph theory, but it has also been found that some hydrogen bonding systems obey density scaling,[8,11,21] though possibly in a restricted density range and generally with very low values of γ (around 1).

Ionic liquids are a class of liquids that have received enormous attention in the last two decades, primarily because of their promise in applications.[22] They also represent an important category of liquid worthy of study for fundamental reasons: in particular, with modern room-temperature ionic liquids, the Coulomb interactions are diluted due to the large size of the molecules. Therefore, it makes sense to consider them as an intermediate case between van der Waals liquids and strongly ionic liquids such as the classical molten salts (e.g., NaCl). There is experimental data demonstrating density scaling for the different transport coefficients (viscosity, electrical conductivity, and self-diffusion) in many different ionic liquids.[23–33] In addition, recent experimental work[34] showed that the time scale and spectral shape of the main (slow) dynamical process at microscopic scales, seen in neutron spectroscopy, are also invariant along the same lines as the conductivity for Pyr14TFSI. Moreover, these authors also examined the structure factor as measured using x rays and found that it was partly invariant: the so-called charge peak reflecting charge ordering varied slightly along isoconductivity lines, while the main peak at large wavenumbers was quite invariant. The density changes involved were small, of order 2%. Therefore, Pyr14TFSI does not have isomorphs since not all of the microscopic structure is invariant, although certain aspects are. If one subscribes to the notion that dynamics and structure must be related, in that structure, or some particular aspect of it, governs dynamics, then it is not surprising that at least part of the structure is invariant along the isoconductivity lines. This reasoning has been called, in the context of isomorph theory, the isomorph filter,[12] and a generalized version of it applies here: if one should claim that some aspect of structure should "control" the dynamics, then that aspect must be invariant along the same curves that dynamics is. If one does not know which aspect of structure is controlling the dynamics, one should start by searching among those aspects that are invariant along those lines. In this work, we include a limited analysis of structure, and a more detailed discussion can be found in Ref. 35.

In previous work, we studied by simulation a simple model of a molten salt[36] over a large density range. The wide range allowed us to effectively vary the strength of the Coulomb interactions; at high densities, they become less relevant compared to the other interactions due to the relatively slow rise of the Coulomb potential at short distances. In that work, dynamics and structure were studied along curves of constant excess entropy, which according to isomorph theory, are isomorphs, assuming these exist.[12,37] Curves of constant excess entropy—which always exist—are referred to as configurational adiabats. A remarkable contrast was revealed between dynamic invariance along configurational adiabats on the one hand and substantial variation of structure on the other hand. When restricting to moderate density changes and considering the structure factor, a similar picture to that reported by Hansen *et al.* was found, namely a near invariance of the main peak together with a variation in the charge peak. However, the larger picture can be expressed as the contrast between near-invariant dynamics and non-invariant structure. This contrast was striking enough to justify coining new terminology: we designated curves along which dynamics are invariant as *isodynes*. Clearly, by this definition, isomorphs are isodynes, but the reverse is not generally true, as has also become evident in some recent publications.[38–40] We note that early simulation work on density scaling in charged systems seemed to indicate that the presence of charges prevented good density scaling,[41] although only power-law density scaling was attempted, and the charges were rather large in that case. Our 2021 work on a simple molten salt shows that a regime exists where the charges are strong enough to have non-trivial effects, but good isodynes can nevertheless be observed. On a related matter, it has proved difficult to establish corresponding state equations for molten salts because the van der Waals and electrostatic terms in the potential are not mutually scalable in the same way,[42] although recent works have studied the applicability of entropy scaling for simple monovalent salts[43] and ionic liquids.[44]

In the absence of isomorphs, we lack a theoretical foundation to explain the existence of isodynes, which is in fact rather puzzling and an open question. In simple liquids, it is likely related to the phenomenon of excess-entropy scaling.[45,46] For more complex molecular liquids, the answer will presumably somehow involve understanding in a coarse-grained sense which aspects of the microscopic structure are actually relevant for the dynamics of interest,[47] but the question also stands for the simple molten salt model studied in our previous work, where coarse graining would not seem to be a relevant strategy. In addition, there is no theoretical ground for assuming any particular scaling form: the argument of the function f in Eq. (1) is not required to have the form $h(\rho)/T$ but could have, for example, the form $\rho/h'(T)$, as we shall see later. The approach taken in this work is, therefore, to focus on identifying curves of invariant dynamics. Whether a suitable scaling variable can be identified for a density scaling analysis is an interesting but separate question.

The purpose of this work is to study, by simulation, a realistic model of an ionic liquid that has been demonstrated to have isodynes experimentally. If the simulated system likewise has isodynes, it offers the possibility to study these isodynes in much more detail than what can be performed experimentally. The specific aim is thus (1) to determine to what extent isodynes exist in the simulated ionic liquid, (2) to characterize their shape in the phase diagram, in particular the value(s) of the density scaling exponent γ, and (3) to document which aspects of microscopic dynamics are indeed invariant along the identified isodynes. The strategy is as follows.

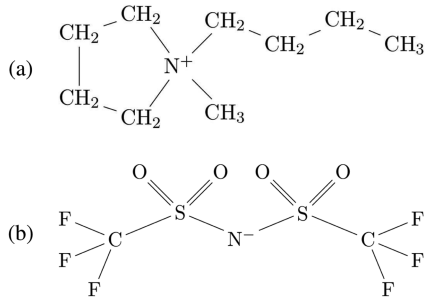

FIG. 1. Visual representation of the molecular structures of the (a) cation, 1-butyl-1-methylpyrrolidinium (Pyr14), and (b) anion, bis(trifluoromethyl)sulfonylamide (TFSI), simulated in this work.

For item 1, we focus initially on the viscosity and the diffusion coefficient(s). Comparing contour plots of these quantities (appropriately scaled; what we refer to below as "reduced units") will give the first indications of isodynes. A series of simulations along putative isodynes chosen as, for example, viscosity contours allows direct checks of the invariance of other quantities, including orientational dynamics.

The system we investigate in this work has the full name 1-butyl-1-methylpyrrolidinium bis(trifluoromethyl)sulfonylamide. We abbreviate the cation as Pyr14; it has a molar mass of 142.257 g/mol and is also referred to in the literature as C_4MPYRR (the M standing for methyl). The anion, which we abbreviate as TFSI, has a molar mass of 280.143 g/mol and is also referred to in the literature as NTF_2. The total molar mass is thus 422.4 g/mol. Both ions have appeared in many studies on ILs; the cation is often part of a series Pyr1*n*, where *n*, equal to four in our case, is the number of carbon units on the tail. The cation and anion are shown schematically in Fig. 1. Pyrrolidinium ILs are used in electrochemical applications because of their wide electrochemical windows and high electrochemical stability.[22]

The structure of the paper is as follows. Section II gives details of the liquid to be studied and of the simulation model and potential. Section III gives an overview of the simulations and includes some comparisons with experimental data. In Sec. IV, we present our procedure for identifying isodynes and describe our main results, namely the presentation of dynamical data for different isodynes. Section V discusses the significance of the results in terms of the larger question of how widespread isodynes are. It also discusses how the concept of coarse-graining is connected to the existence of isodynes in complex molecular systems. Section VI offers some perspectives for future work.

II. MODEL AND POTENTIAL

For most of our results, we use a united-atom model for the Pyr14 cation, i.e., representing each CH_2 or CH_3 group as a single sphere in order to reduce the number of degrees of freedom and to increase the time step (due to not having to resolve the CH bond vibration). There are no H atoms on TFSI, so there is no possible simplification by using united atoms there. Comparison between all-atom and united-atom models shows that the latter tends to be less viscous, in general, with viscosities typically lower by factors 2–3 than the corresponding all-atom models.[48] This does not mean that the all-atom viscosity is necessarily closer to experimental values; however, force field parameters should always be selected to provide the most accurate representation of densities and viscosities for the system under consideration.

We use literature parameters coming from the OPLS family of all-atom molecular force fields,[49–51] which we have adapted as necessary to our UA model. The increased interest in ionic liquids has also led to the development of OPLS extensions for this class of liquids.[52,53] For our system, the earliest set of OPLS parameters for the anion (TFSI) we have found is in Ref. 54, which provides all non-bonded interactions (including partial charges) and all bonded interactions (bonds, angles, and dihedrals). For our cation (Pyr_{14}), we used the parameters from Xing *et al.*,[55] who used standard bonded and non-bonded parameters from Refs. 56 and 57. Furthermore, Xing *et al.*[55] obtained the partial charges from the optimized geometry using the RESP method with the R.E.D.-III.4 package. We have adapted these all-atom literature parameters to make corresponding united-atom potentials. To make a united-atom model of the molecule, we replace the CH_2 and CH_3 groups in Pyr_{14} with Lennard-Jones spheres, with the non-bonded parameters for these taken from Refs. 58 and 59. The partial charges of the united atoms are simply the total charges of the relevant C and H atoms. To account for polarizability effects in a simple way, we scale all partial charges by a factor of 0.8;[53] this is discussed in the supplementary material. We use the unit system where lengths are in Angstrom (Å), energies are in kcal/mol, masses are in Dalton (u), and charges are in units of the elementary charge (e). Molecular number densities (total number of ions per unit volume) are expressed in nm^{-3} rather than $Å^{-3}$ for convenience, however.

Some technical differences from the usual OPLS implementations should be noted. The interactions are truncated via the shifted-force method, which is applied at 2.5σ for each interaction rather than having a common absolute cutoff distance. We also use this cutoff method for the electrostatic (Coulomb) interactions, omitting the long-range part of these (see the supplementary material). Second, we use Lorentz–Bertholot mixing rules rather than purely geometric rules, as is standard with OPLS potentials. Finally, we exclude non-bonding interactions for all atoms involved in a dihedral interaction rather than applying a 0.5 weighting for the extreme atoms (1 and 4), as is standard in OPLS. The differences presumably have some effect on the pressure (and possibly the bulk modulus), meaning it is wise to be cautious when comparing the simulation-derived pressures with experimental data. While the choice of mixing rules has been shown to have an effect on the solubility of NaCl in water,[60] such effects are not expected to be relevant or significant in the present case. All simulations in this work were performed with *Roskilde University Molecular Dynamics* (RUMD), Version 3.5.[61] We have carried out a limited number of simulations using an all-atom model. The most interesting question here is whether isodynes of the united-atom model are also isodynes in the AA-model, which can be determined by simulating the AA model on state points identified as being isodynes of the UA model.

III. SIMULATIONS

A. Simulated region of the phase diagram

Figure 2 shows the part of the density temperature phase diagram we have simulated. The overall region of interest in the phase diagram can be defined by three criteria, which are: (1) requiring positive pressure, which defines a boundary with a negative slope on the low-density side, close to the liquid–gas coexistence curve, the region thus excluded being colored gray; (2) relaxation times accessible to simulation, allowing the determination of equilibrium properties within reasonable times, which defines a boundary with a positive slope on the high-density side, corresponding to a version of the glass transition line, the region excluded being colored red; and (3) an upper temperature limit, in principle corresponding to the limit of thermal stability of the molecules. For criterion (1), we use the uncorrected pressure of the model; we estimated the corrected pressure would be about 10 MPa lower due to the long-range part of the Coulomb interaction (though there are other uncertainties in the pressure), such that the zero-pressure line would exclude a greater part of the phase diagram. For criterion (2), we define a timescale τ_{F_s} from the self-intermediate scattering function curve (F_s) for the N-atom on the cation (N^+) as the time at which the F_s reaches a value of e^{-1} of its initial value. The criterion in the phase diagram is that τ_{F_s} = 1 ns. Regarding criterion (3), the thermal stability of ionic liquids has been extensively studied; the so-called onset temperature (at ambient) pressure is typically between 450 and 750 K.[62] For our liquid, the onset temperature has been measured at 724 K.[62] Given that our model cannot decompose thermally anyway, we choose to extend this limit somewhat, up to 1000 K; studying it over a broader temperature range allows us to get a clearer idea of its overall behavior. For orientation, we note that the critical point has been estimated for this IL to be around density 0.57 nm^{-3} and temperature 1050 K,[63] thus well to the left and at a higher temperature than the points shown.

B. Comparison with experiment: Equation of state and viscosity

To find out how well the model resembles reality, we compare pressure, diffusion coefficient, and viscosity with experimental data from Harris *et al.*[64] The diffusion coefficient data were only provided as a function of pressure; given the systematic uncertainties in the simulated pressure discussed earlier, for comparison, we determined the experimental densities using the equation of state from Ref. 34, where the Tait equation was used. A consistency check with the data in Ref. 64 shows that the uncertainty on the determined experimental densities is of order 0.3%. Therefore, we can plot the experimental data together with the simulation data as a function of density on isotherms.

To assess the systematic errors in our simulated pressure, we compare it with the experimental data (see Fig. 3). Our simulated pressures are generally greater than the experimental ones, by up to 20 MPa, when comparing data at equal temperature; the overall pressure range of our simulated data is comparable with that of the experimental data, however. The simulated slopes are smaller than the experimental ones, indicating a bulk modulus roughly 10%–20% smaller. These discrepancies are at least partly due to the cutoff, not least regarding the long-range part of the Coulomb interactions. It is possible that the curves converge (rather than cross) at even higher densities, meaning that the missing part of the pressure becomes less important at higher densities.

When comparing the diffusion coefficient, we consider the two isotherms T = 50 and 75 °C [see Fig. 4(a)]. The simulated and experimental data are in a similar range, with the simulations generally being faster (by factors of order 1.5–2). The deviation is larger for the lower temperature. The data are nearly exponential in density, with remarkably similar slopes in the semi-log representation, differing only by a few percent both between isotherms and between experiment and model.

Figure 4(b) shows the comparison of the viscosity between the simulations and experiments. As before, experimental and simulated values are comparable, with the simulated viscosity being lower by factors up to 3. Considering data for 50 and 75 °C, the discrepancies are quite similar to those for the diffusion coefficient, indicating that the simulated liquid's dynamics are overall faster by factors of order 2 and 1.5 than the corresponding experimental system, respectively, for these temperatures. Moreover, it is also clear here that the discrepancy grows as temperature decreases to even lower values, while the density dependence is remarkably similar across temperatures and between experiment and model. The combination of differences

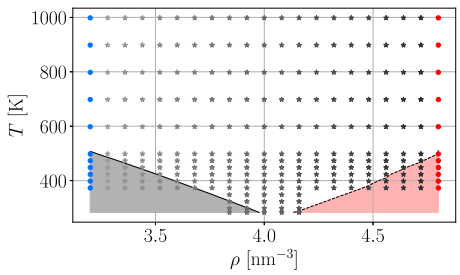

FIG. 2. Density-temperature phase diagram showing simulated points. The boundary curve on the lower left represents zero pressure, and that on the lower right represents impractically slow dynamics, determined by the criterion that it takes 1 ns for the self-intermediate scattering function of N^+ to reach a value of e^{-1}. The q in the self-intermediate scattering function was chosen to be the position of the main structure factor peak. For our simulations, it is between 0.7 and 0.9 $Å^{-1}$.

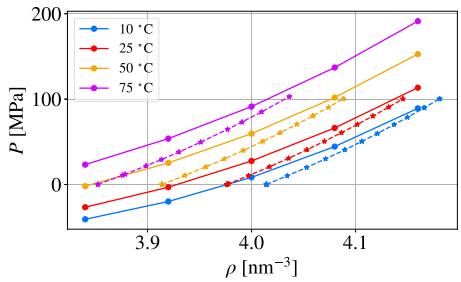

FIG. 3. Simulated pressure-density isotherms (dots, solid lines) compared with experimental data from Harris *et al.*[64] (stars, dashed lines). Statistical errors on the simulation data have been estimated using standard methods, determining the number of independent samples based on the time taken for the pressure autocorrelation to fall below 5% of its initial value. The errors are of order 0.5 MPa and, in all cases, smaller than the symbol size.

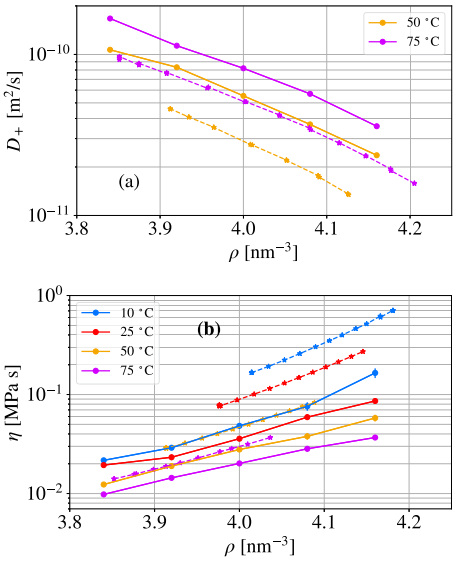

FIG. 4. Simulated transport coefficients (dots, solid lines) compared with experimental data of Harris *et al.*[64] (stars, dashed lines): (a) diffusion coefficients of the cation D_+ as a function of ρ; (b) η as a function of ρ.

and similarities has consequences for the density scaling exponent, as will be discussed below.

IV. DYNAMICS AND ISODYNES

A. Reduced units

In our earlier study,[36] we used isomorph theory to analyze the simple salt model of Hansen and McDonald.[65] We found lines in the $\rho - T$ phase diagram where the dynamics are invariant when scaled according to the isomorph theory. This scaling, introduced by Rosenfeld,[66] uses thermodynamic properties such as number density ρ and temperature T so that the scaled quantity becomes dimensionless. These reduced quantities are symbolized by a tilde. Therefore, a distance r in reduced units becomes $\tilde{r} = \rho^{1/3} r$. The three fundamental scaling factors, along with two derived ones, can be found in Table I. A more detailed list of scaling factors for isomorph scaling may be found in Gnan *et al.*[12] The same scaling of quantities to make them non-dimensional has been used by Dymond *et al.*, who were inspired by a hard-sphere-type modeling scheme (see, for example, Refs. 4 and 67).

B. Determining isodynes using viscosity and diffusion coefficient

Figure 5 shows our data for the cation diffusion coefficient and the inverse viscosity (also known as fluidity). Fits to second and third-order polynomials as a function of temperature for each simulated density are also shown. The diffusivity data included more scatter, and a third-order polynomial was observed to overfit the data. The reason for the scatter is likely the relatively small number (200) of cations in the simulation, leading to statistics that are poorer than usual for simulated liquids. These fits were obtained primarily

TABLE I. List of scaling factors for isomorph scaling. The first three, energy, length, and time, can be considered fundamental (alternatively, mass can be taken as fundamental); all others can be derived from these three essentially by dimensional analysis.

Dimension	Scaling factor	Reduced quantity
Length	$l_0 = \rho^{-1/3}$	$\tilde{l} = l/l_0$
Energy	$E_0 = k_B T$	$\tilde{E} = E/E_0$
Time	$t_0 = \rho^{-1/3}\sqrt{\frac{m}{k_B T}}$	$\tilde{t} = t/t_0$
Diffusivity	l_0^2/t_0	$\tilde{D} = D\rho^{1/3}(k_B T/m)^{-1/2}$
Viscosity	$E_0 t_0/l_0^3$	$\tilde{\eta} = \eta\rho^{-2/3}(m k_B T)^{-1/2}$

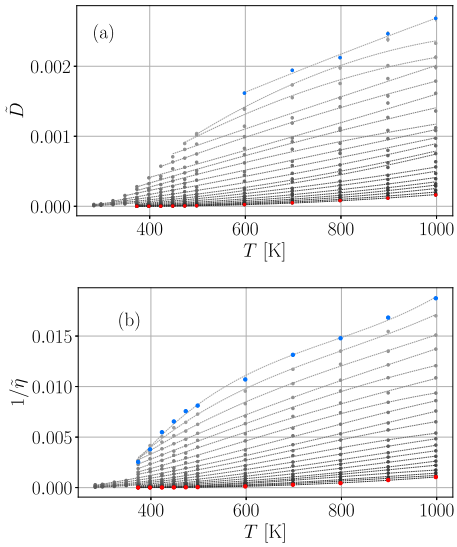

FIG. 5. Fits of (a) reduced diffusion coefficient for cations (specifically the N^+ atom) $\tilde{D}$ and fits to a second-order polynomial and (b) the fluidity, or inverse viscosity $1/\tilde{\eta}$, as a function of temperature for different densities, together with fits to a third-order polynomial. The colors correspond also to the points shown in Fig. 2. Data for the lowest and highest densities are plotted in blue and red, respectively (see Fig. 2).

for the purpose of interpolation so that the contours of $\tilde{D}$ and $\tilde{\eta}$ could be identified.

Contour plots showing selected contours of D and η are shown in Fig. 6(a), while contours of the reduced quantities $\tilde{D}$ and $\tilde{\eta}$ are given in Fig. 6(b). These plots were generated from a grid of values using a standard algorithm.[68] The contour values have been chosen to make approximately coincident contours of the two quantities at $T = 598$ K. It is clear that the two sets of contours for the nonreduced quantities do not coincide, while those for the reduced quantities match remarkably well. The black curves (diffusivity) appear to be systematically slightly steeper, though this difference is barely larger than the apparent noise. Therefore, we can identify these common contours as *isodynes* or curves of invariant dynamics (in reduced units).

For further investigation, we choose specifically to work with contours of reduced viscosity to generate isodynes. New simulations were then run at densities and temperatures along several different

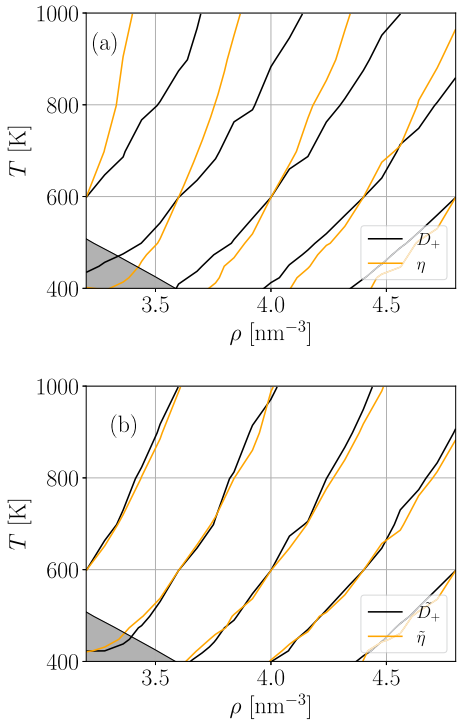

FIG. 6. Contours of diffusivity and shear viscosity in the ρ-T diagram in (a) standard units and (b) reduced units. The contours were chosen to pass through the following points: ρ = 3.2; 3.6; 4.0; 4.4; 4.8 nm^{-3}, all at T = 598.15 K.

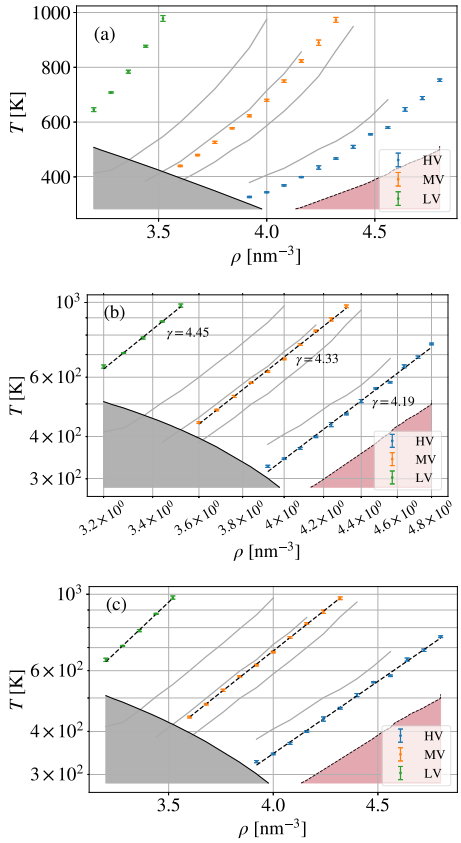

FIG. 7. Selected isodynes shown in (a) lin–lin, (b) log–log, and (c) log–lin plots. Power-law and exponential fits are included in (b) and (c), respectively. The colored points indicated the three isodynes HV ($\tilde{\eta}$ = 2693.0), MV ($\tilde{\eta}$ = 336.6), and LV ($\tilde{\eta}$ = 84.2) that we focused on in the analysis, while the gray ones indicated other isodynes on which simulations had been run. For the power-law fits, the values of the density scaling exponent γ are shown by each curve.

isodynes. For generating these contours of reduced viscosity, we rely on the fits shown in Fig. 5. For a given value of reduced viscosity (or inverse reduced viscosity) and for each density, the corresponding temperature was found by interpolation. The covariance matrix from the polynomial fits was used to construct error bars for the temperature. In the analysis below, we focus primarily on three isodynes, labeled HV, MV, and LV for high, medium, and low (reduced) viscosity, respectively, and chosen to cover a broad region of the phase diagram. The other isodynes that have been simulated are shown in gray in the figures. Before presenting simulation data along the isodynes, we discuss their shapes in Subsection IV C, which is further illuminated by a density-scaling analysis in Subsection IV D and followed by a discussion of the relevance of the Stokes-Einstein (SE) relation to isodynes in Subsection IV E.

C. The shape of isodynes

The existence of common invariant curves for two (or more) different dynamical quantities does not by itself imply the scaling form Eq. (1), which has to be determined from an analysis of their shapes. Figures 7(a)–7(c) show selected isodynes on linear, double logarithmic, and semi-logarithmic scales, respectively. In panel (b), power-law fits are included, with the exponents γ indicated. The γ values are in the fairly narrow range of 4.3–4.4, seemingly higher for higher temperatures and lower densities. Alternatively, the contours can be fitted using exponential functions,

$$T(\rho) = T_0 \exp(b\rho), \tag{2}$$

the density scaling exponent γ is then no longer constant along a given isodyne but is defined as the logarithmic derivative

$$\gamma(\rho) \equiv \frac{d \ln h(\rho)}{d \ln \rho} = b\rho = \ln\left(\frac{T}{T_0}\right). \tag{3}$$

The exponential fits are shown in Fig. 7(c). They are slightly better than the power-law fits (around a factor of two reduction in χ^2). Apart from fitting the isodynes better, the exponential fits give a more complete picture of how γ varies in the phase diagram. Along a given isodyne, one can express γ as a function of either ρ or T, as indicated in Eq. (3). However, γ can be defined at any point in the ρ, T-plane as the logarithmic slope of whichever isodyne passes through that point, and in general, it is a function of both ρ and T. We can get a sense of how much γ depends primarily on ρ or T by plotting the fitted values of γ as a function of each separately. Figures 8(a) and 8(b) show plots of γ vs density for each isodyne vs ρ and T, respectively. Greater variation of γ overall is apparent than was seen in the power-law fits, covering values between 3.8 and 4.8 [the constant values of γ from the power-law fits are also

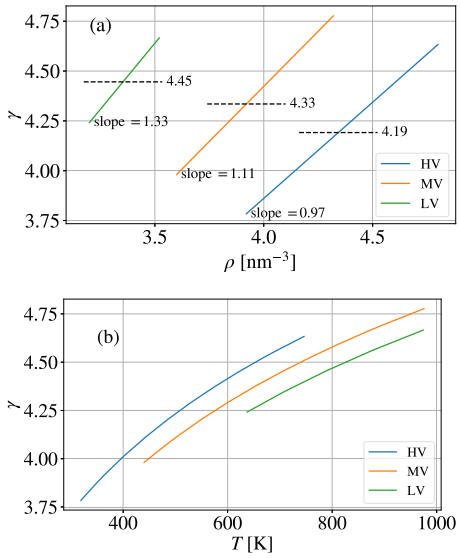

FIG. 8. Density scaling exponent γ from exponential fits to isodynes plotted as a function of (a) ρ and (b) T. The values of the b parameter are indicated in the figure. The values of the parameter T_0 were 7.26, 8.22, and 9.16 for HV, MV, and LV, respectively.

shown in Fig. 8(a) for comparison]. Moreover, it is clear from the approximate collapse visible in Fig. 8(b) that γ depends primarily on T and relatively little on ρ if T is held fixed. In terms of the fit parameters T_0 and b from the exponential fit, this means that T_0 depends rather little on which isodyne is considered, while b varies significantly.

The experimental density scaling exponent for this system was determined to have significantly lower values, in the range of 2.8–3.0,[34] than what we see. Some of the difference can be explained by the lower temperatures in the experimental measurements (<310 K), but no reasonable extrapolation of the blue curve, say, will take γ down to 3 at T = 300 K. The greater values of γ in the model are, however, consistent with the observations made above in comparing experimental and simulated data for the diffusion coefficient and viscosity (see Sec. III B, Fig. 4). There, it was noted that the density dependence was rather uniform, both across different isotherms and between experimental and simulated data, while the temperature dependence differs between experiment and model. In particular, the viscosity increases more rapidly upon cooling at a fixed density for the experimental system than for the model. This is equivalent to a smaller γ for the experimental case by the following argument: for a given ρ, T starting point, a given increase in ρ increases both the experimental and model (reduced) viscosity by the same fractional amount. To compensate for this and return to the starting contour, the temperature must be decreased. Because the experimental system is more sensitive to temperature (at a fixed density), a smaller temperature change is required, corresponding to a smaller γ. This reasoning makes use of the fact that a given increase in density gives essentially the same factor increase in viscosity in both the real and the model systems.

D. Density scaling analysis

The concept of isodynes is closely related to that of density scaling, as mentioned in the introduction. Traditionally, density scaling has been illustrated by plotting the putative invariant quantity as a function of some scaling variable Γ. For the simplest case, $\Gamma = \rho^{\gamma_0}/T$, corresponding to power-law isodynes $T \propto \rho^{\gamma_0}$ (the subscript 0 on γ is to emphasize that this is a fixed parameter). For an expression that can account for the variation of γ with temperature, we can use the exponential fits from above, recalling that the parameter T_0 was relatively insensitive to the choice of isodyne. Taking the last expression for γ in Eq. (3) as a general expression for $\gamma(\rho, T)$,

$$\gamma(\rho, T) = \ln\left(\frac{T}{T_0}\right), \tag{4}$$

gives isodynes with the form Eq. (2), with a common value of T_0 but different values of b. The latter, or more conveniently, its reciprocal, is, therefore, a natural choice of scaling variable (an index that can distinguish different isodynes) and can be expressed in terms of ρ and T as

$$\Gamma \equiv b^{-1} = \frac{\rho}{\ln(T/T_0)}. \tag{5}$$

The parameter T_0 is, in this formulation, a characteristic temperature for the material. Figure 9 shows density scaling plots for reduced viscosity and reduced diffusivity, respectively. The state points used here are those plotted in Fig. 2, i.e., the grid of points used for the initial simulations from which isodynes were identified. In each case, the blue points show the case of power-law density scaling, and we have chosen γ_0 = 4.3 as a representative value from the middle of

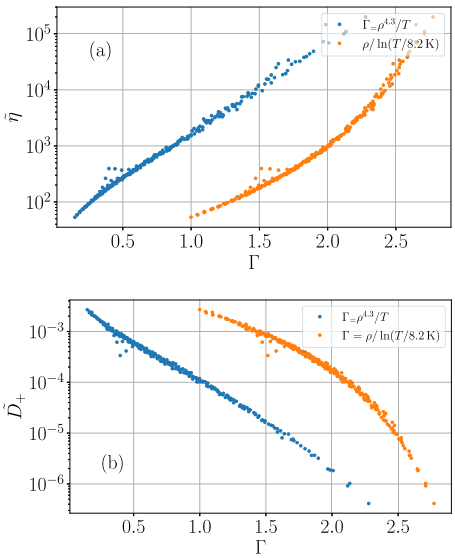

FIG. 9. Density scaling plot for (a) reduced viscosity and (b) cation diffusivity. Two choices of scaling variable Γ are used [see Eq. (5)]: one corresponding to ordinary density scaling ($\Gamma = \rho^{\gamma_0}/T$) and one corresponding to the T-dependent γ, namely $\Gamma = \rho/\ln(T/T_0)$, with T_0 to be 8.2 K from the parameters for the middle curve in Fig. 8. What is plotted is actually 3Γ − 1 to spread the data out on the x-axis to make it easier to compare the degree of collapse in the two cases.

the region of interest [Fig. 8(a)]. The orange points show the choice $\Gamma = \rho/\ln(T/T_0)$ with $T_0 = 8.2$ K, based on the fit to the middle curve (MV) in Fig. 8. Both choices give reasonably similar scaling collapses of the data. This shows that smaller errors are required to be able to conclude anything about γ and its temperature or density dependence using a density-scaling analysis.

The weak (i.e., logarithmic here) temperature dependence of γ, as evident in Eq. (3), may be a generic feature of ionic liquids. Molten salts are often referred to as high temperature liquids for obvious reasons. However, in regard to their physical properties, they are perhaps better described as "low temperature" liquids in a statistical mechanical sense as $k_BT/\varepsilon \ll 1$, where ε is the well-depth at contact of the excluded volumes because of the very large magnitude of the Coulomb energy in units of ambient values of k_BT at typical charge separations in the system. This is illustrated by, for example, the very low value of the critical temperature ($T_c^* \simeq 0.05$) of the Restricted Primitive Model (RPM) of an ionic liquid.[69] This might lead one to conclude that the Coulombic terms in ionic liquids might be treatable for practical purposes as a uniform background that just shifts the macroscopic unit collapse curves and that the basic transport coefficient expressions found for neutral polyatomic liquids (e.g., by Dymond *et al.*) might also apply to a large extent to the present systems, as may be inferred from the data trends in Fig. 9.

E. Stokes–Einstein relation

Diffusivity and viscosity are often assumed to be related through the so-called Stokes–Einstein (SE) relation,[70] and deviations from it are considered noteworthy, as in the case of several IL simulations.[71–74] It is, therefore, important to investigate to what extent the SE relation is compatible with the existence of isodynes. The connection between the SE relation and isomorph theory has been explored recently and suggests a reformulation of the SE relation.[75] To test the standard SE relation, Fig. 10(a) shows the effective hydrodynamic diameter,

$$\sigma_H = \frac{k_BT}{2\pi D\eta}, \tag{6}$$

for state points on all simulated isodynes (the coefficient 2 in the denominator applies for slip boundary conditions). The value of σ_H would be constant if the standard Stokes–Einstein relation were strictly valid, as for a macroscopic hard sphere diffusing in a viscous liquid. Here, the hydrodynamic diameter is seen to decrease, albeit weakly, with increasing density.

A modification of the original Stokes–Einstein relationship at the microscopic scale[70] was made by Zwanzig, who derived a hydrodynamic diameter given by $\rho^{-1/3}$, using a semi-empirical quasi-lattice model for the dynamics of the liquid molecules,[76–79] following earlier works.[80,81] The Zwanzig version of the SE formula is given by the identity, $\tilde{\eta}\tilde{D} = const$. The same conclusion was made by Costigliola *et al.*,[75] who noted that this formulation is more compatible with isomorph theory. Indeed, the Stokes–Einstein (SE) relationship written in isomorph (reduced) units is

$$\tilde{D}\tilde{\eta} = \frac{1}{c\pi\tilde{\sigma}_h}, \qquad \tilde{D}\tilde{\eta} = \alpha = \frac{1}{c\pi}, \quad \text{if} \quad \tilde{\sigma}_h = 1, \tag{7}$$

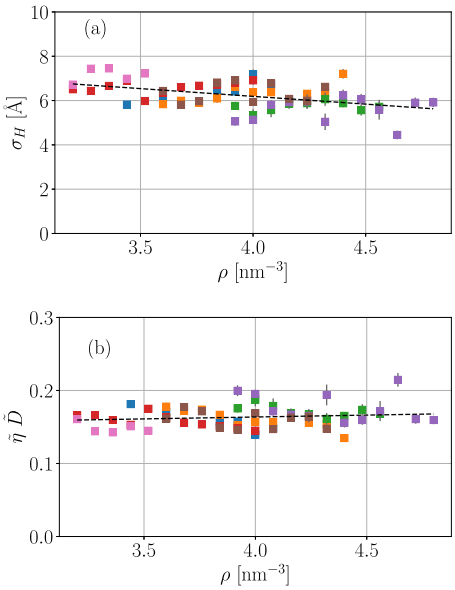

FIG. 10. Test of the Stokes–Einstein relation, data from the simulated isodynes. (a) Effective hydrodynamic diameter; (b) the dimensionless quantity $\tilde{\eta}\tilde{D}$, which is involved in the isomorph-compatible version of the reduced Stokes–Einstein relation. The colors indicate points on different isodynes.

where the characteristic diameter is $\tilde{\sigma}_H = \sigma_H\rho^{1/3}$. The constants $c = 2$ and 3 correspond to slip and stick boundary conditions. Therefore, the SE constant $\alpha = 1/c\pi = 0.159$ and 0.106 for slip and stick boundary conditions, respectively, where $\tilde{\sigma}_H = 1$ at all state points is taken (i.e., the Zwanzig result). Note that in Eq. (7), when the SE is expressed in isomorph units, it is evident that there is no temperature dependence of the SE constant, α.

Figure 10(b) shows the dimensionless quantity $\alpha = \tilde{\eta}\tilde{D}$. It is clear that this is a better candidate for an invariant quantity reflecting molecular dynamics in the framework of isomorph theory.[75] Isomorph theory does not require α to be constant, but it can be collapsed as a function of temperature on a single curve. At low to moderate temperatures, α approaches a constant value, which for the Lennard-Jones (LJ) fluid, for example, is observed to be 0.146.[75] Values of α at high density are ~0.15 for LJ, 0.17 for hard spheres, and 0.14 for the one-component plasma and Yukawa ($\kappa = 2$) potential systems,[82] and for TIP4/ice water, $\alpha = 0.15 \pm 0.02$.[83] Our data are consistent with a constant value in the range 0.15–0.20 and, therefore, consistent with these other studies on model systems and the results of Costigliola *et al.*,[75] suggesting the possibility that this quantity is largely invariant across a range of different chemical systems.

The physical content of the "isomorph-compatible," or the Zwanzig version of the Stokes–Einstein relation, is that the effective hydrodynamic diameter refers not to a fixed molecular size but rather to the space available for a molecule to occupy, which is determined by the density. The existence of isodynes implies that $\tilde{\eta}\tilde{D}$ is constant along any given isodyne, but that by itself does not imply that the constant is independent of which isodyne is considered. Therefore, the collapse to a single value (within the

simulation statistics), which is consistent with the isomorph version of the SE relation, is a stronger result.

F. Simulations along proposed isodynes

In this and the following subsections, data from simulations carried out on the proposed isodynes are presented. The isodynes were identified as described in Subsection IV B.

The viscosity, self-diffusion coefficient, and other dynamical quantities are investigated to discover the extent to which they exhibit invariant dynamics. Figure 11 shows the values of the reduced diffusion coefficient and viscosity along the simulated isodynes. The resulting curves are reasonably flat, which confirms the validity of the procedure for determining the contours. The visible variations are larger than the statistical errors, though, which may result from the uncertainties in locating precisely the isodynes in the fitting process.

We have seen that the density scaling exponent of our united-atom model is larger than the value determined experimentally for this IL. A possible reason is the effect of the hydrogen atoms on the temperature dependence of the dynamics. To test for such differences, we have carried out a limited number of simulations of an all-atom (AA) model of the same liquid. Details of the AA model can be found in Ref. 35. Rather than repeating the generation of isodynes from scratch, we have simulated the AA along the isodyne points identified for the UA model. The diffusivity and inverse viscosity in reduced units are shown along isodyne HV in Fig. 12, where they are compared to the corresponding data for the UA model. As expected, the AA model is slower to evolve, showing lower diffusivity and fluidity by factors of 2–3. The statistical error in the AA data is also smaller, allowing a slight downward trend to be discerned.

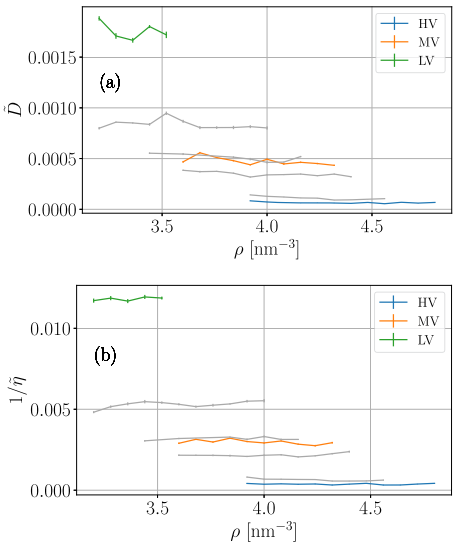

FIG. 11. Dynamics along all simulated isodynes in scaled units. The colored ones are the three main simulated isodynes we have focused on. The gray ones are other isodynes we simulated but have not studied in detail. They are included here as extra checks that our procedure yields reasonably invariant dynamics along isodynes. (a) Scaled diffusion coefficient for N^+ in the cation, and (b) scaled inverse viscosity (fluidity).

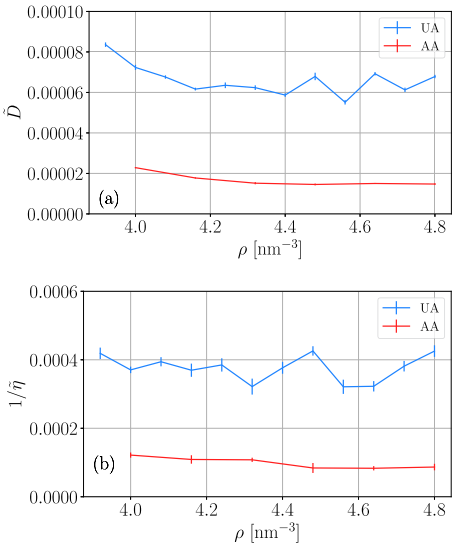

FIG. 12. Comparison of dynamics between the united-atom (UA) and all-atom (AA) models along isodyne HV in scaled units. (a) Scaled diffusion coefficient for N^+ in the cation, and (b) scaled inverse viscosity (fluidity).

However, this trend is consistent with the data for the UA model, and the quantities shown do not vary more for the AA model than they do for the UA model. This excludes the absence of H atoms from being the cause of the higher γ in the simulations.

To go beyond the scalar quantities $\tilde{D}$ and $\tilde{\eta}$, the time-dependent functions from which they are derived are explored. These include the mean-square displacement (MSD) of N^+ and the shear stress autocorrelation function. These are shown along isodyne MV and the isotherm $T = 598$ K in Fig. 13. There is good collapse for the MSD [panel (a) of the figure], apart from a region at short times where presumably some internal dynamics, not invariant in reduced units, is active. Data for the isotherm $T = 598$ K are shown for comparison. For the stress autocorrelation function [panel (b) of the figure], there is also a quite good collapse, particularly when compared to the isothermal data. Some variation is visible at small and intermediate times. In particular, the small oscillations at intermediate times of 1–10 reduced units vary slightly along the isodyne. In fact, in nonreduced units, these are aligned in time (data not shown); these are presumably associated with particular internal motions that are not particularly coupled to the overall molecular dynamics and have their own fixed characteristic time scales.

This paper focuses on dynamics rather than structure. Nevertheless, before continuing our investigation of dynamical invariance in Sec. IV G with rotational dynamics, it is worth making the point that the curves identified here are *isodynes* rather than *isomorphs*. To this end, we show the x-ray structure factor along the isodyne MV in Fig. 14(a).

It is clear that the structure is far from invariant. It is also clear that most of the variation is in the low-q "charge-ordering" peak. Indeed, showing $S(q)$ for only two nearby densities in Fig. 14(b) reveals this contrast more strikingly: for small density changes, the main peak is quite invariant while the charge peak changes visibly,

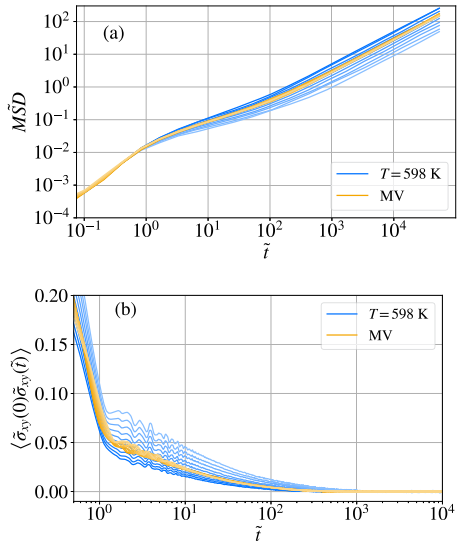

FIG. 13. Reduced-unit MSD (a) and stress autocorrelation (b) along isotherm $T = 598$ K (blue curves) and isodyne MV (orange curves).

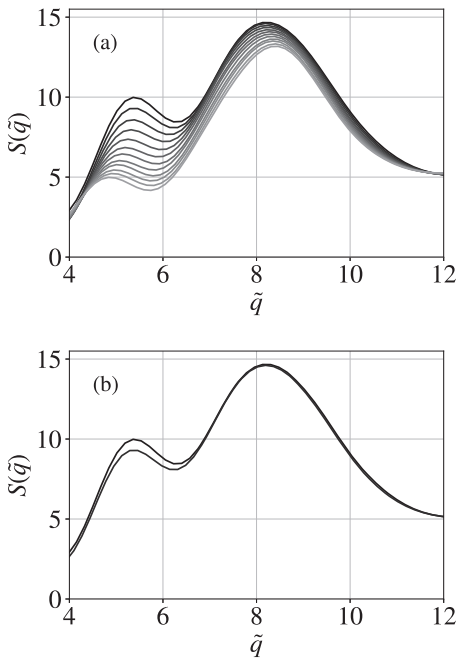

FIG. 14. (a) X-ray structure factor along isodyne HV, calculated by the Fourier transform of the partial radial distribution functions and summing over all pair types with appropriate weights. Shading is darker for lower densities. (b) Same as (a), but including only the lowest two densities, 3.92 and 4.0 nm^{-3}, differing by 2%.

becoming smaller and shifting to a slightly lower q with increasing density. This is precisely what has been observed experimentally for this ionic liquid.[34] The overall point of Fig. 14, however, is that the structure varies substantially along a curve on which dynamics is rather invariant. Furthermore, examples of structural variation along isodynes can be found in Ref. 35, where no aspect of the structure could be identified that is as invariant as the dynamics. This is a strange situation since it is a paradigm in material physics that structure determines dynamics, or at least plays a crucial role. For example, a well-known theory for viscous liquid dynamics, mode-coupling theory, is based entirely on this premise.[84,85]

G. Orientational dynamics along isodynes

To widen the scope of dynamical measures encompassed by isodynes, we study other measures of dynamics, specifically molecular rotations. This is performed by defining a normalized vector $\mathbf{e}(t)$ in terms of the atoms within a given molecule and calculating the time autocorrelation function $P_1(t)$ as the average dot product of this vector with itself at different times,

$$P_1(t) \equiv \langle \vec{v}(t_0) \cdot \vec{v}(t_0 + t) \rangle. \tag{8}$$

Here, the notation P_1 refers to the $l = 1$ Legendre polynomial. Borodin and Smith defined rotational correlation functions more or less similarly in their study of a simulated Pyr13-TFSI ionic liquid, including $P_2(t)$ functions.[86] They were interested in the degree of anisotropy, i.e., differences in relaxation rates between rotations in different directions, and found, not surprisingly, that rotations of vectors aligned with the long axes of the ions are the slowest. Our primary concern is the degree of invariance along isodynes and whether this varies for different rotations. It should be noted that a rotational correlation function defined in this way is sensitive to two components of rotation, namely rotations about any two axes orthogonal to the given vector. Obviously, rotations about the given vector cannot contribute to the decay of the corresponding correlation function. Starting with the cation, we define three vectors as (a) normal to the plane containing N^+ and the two R_1 groups, (b) the vector from N^+ to the point midway between the two R_1 groups, and (c) the vector from N^+ to the end of the tail T_4. The first two vectors are meant to test the rotation of the ring, while the latter is meant to test the rotation of the tail. The corresponding $P_1(t)$ correlation functions are shown in Figs. 15(a)–15(c), respectively, along with molecular diagrams indicating the vectors in the insets. Data for the different state points along the isodyne MV are shown as blue points, while for comparison, data along the isotherm $T = 598$ K are shown in gray. All three correlation functions show invariance, such that the different blue datasets cannot be distinguished. By comparison, the gray isotherm data are spread out, decaying over a broad range of time scales. The overall shapes of the three correlation functions on the isodyne are similar, showing an emergent two-step appearance, with the relaxation time increasing somewhat from (a) to (b) to (c). The degree of invariance is greatest for part (b); for the other two functions, the blue data points show a small degree of spreading.

For the anion, we consider two vectors: (a) the vector from one S atom to the other (due to the molecule's symmetry, the order is irrelevant), and (b) the normal to the plane containing N^- and the two S atoms. The correlation functions are shown in Figs. 16(a) and 16(b), respectively, again from isodyne MV (blue points) and from isotherm $T = 598$ K (gray points). The isodyne data in panel (a) show reasonable invariance, i.e., collapse, although not as striking as that of the cation rotations in Fig. 15. On the other hand, the data in panel (b) vary rather more along the isodyne. In fact, the amount of

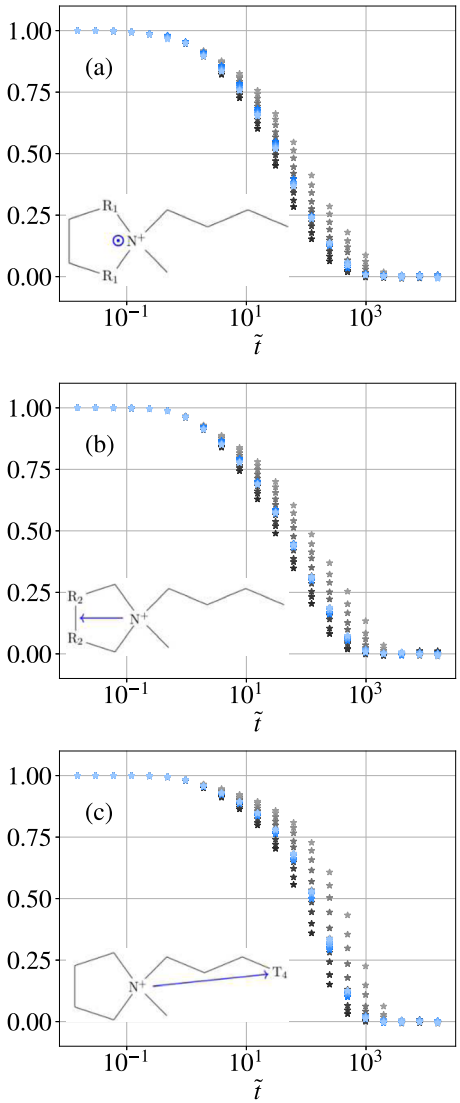

FIG. 15. Orientational dynamics of the cation along isodyne MV, shown in different shades of blue for different densities, together with the same function on the isotherm $T = 598$ K, shown in gray, for more or less the same range of densities. The autocorrelation function of (a) the normal vector to the plane spanned from the two R_1 groups and N^+, (b) the vector from N^+ to the point between the two R_2 groups, and (c) the vector from N^+ to the end of the tail (T_4).

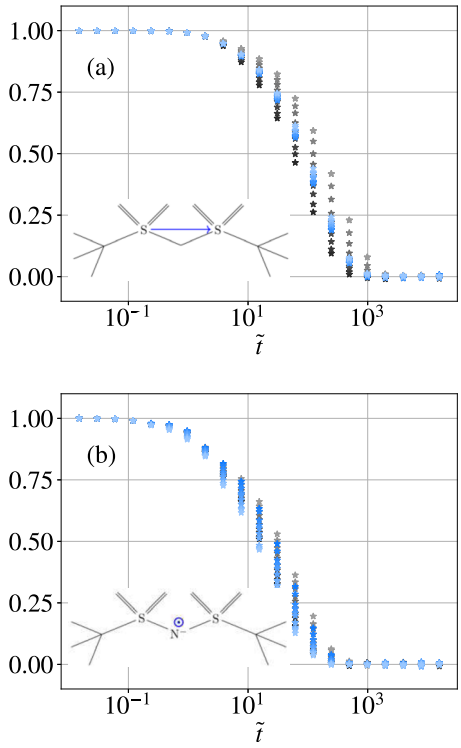

FIG. 16. Orientational dynamics of the anion along isodyne MV. The autocorrelation function of (a) the vector between the two S atoms in the anion and (b) the normal vector to the plane spun from the two S atoms and N^-.

variation is almost comparable to that along the isotherm. This is a striking and noteworthy result: while most of the rotational correlation functions we have investigated show invariance, one does not. The vector involved in the non-invariant rotation is sensitive both to rotations of the anion about its long axis and to one rotation perpendicular to the long axis. The non-invariant behavior must arise from rotations about the long axis; otherwise, it would also be manifested in the other correlation function [panel (a)].

The molecular rotations that show invariance are somehow connected to the other dynamical properties showing invariance along the isodynes, while the rotations that do not must be decoupled from the others and from the other invariant dynamical quantities. From the results of this subsection, we see that the rotations associated with a high moment of inertia are invariant, while the case of non-invariant rotational dynamics involves a low moment of inertia (the long axis of the TFSI anion). This is plausible when considering a molecule's interactions with its neighbors. A rotation with a high moment of inertia would be more likely to be geometrically constrained by interactions with neighboring molecules than one with a low moment of inertia. Indeed, it makes sense that a molecule can rotate more freely about an axis of low moment of inertia without influencing the overall dynamics of the system. The connection between these observations and the other invariant aspects of the dynamics will be discussed below in the context of coarse-graining.

V. DISCUSSION

A. Significance of isodynes

How widespread is the existence of isodynes? In an extensive study,[87–95] Assael, Dymond, and co-workers analyzed experimental data on the transport coefficients (coefficients of self-diffusion, viscosity, and thermal conductivity) for a wide range of liquids (see also Ref. 4). They found correlations between them inspired by the hard spheres model but which are consistent with isomorph theory.

In their approach, the reduced unit form of the transport coefficient is a function of the molecular volume V scaled by a limiting high density reference value $V_0(T)$, where the latter is temperature dependent but does not depend on the quantity in question. This is similar, indeed essentially equivalent, to the isomorph-based analysis by Costigliola *et al.*,[96] where the reduced transport coefficients are functions of $T/T_{\mathrm{ref}}(\rho)$ (i.e., using ρ, equivalently volume, as the parameter for the reference temperature instead of the other way around). Indeed, the Lennard-Jones data for $V_0(T)$ presented by Dymond[67] is consistent with the latter function being an isomorph—a power-law fit of T vs $1/V_0$ gives a good fit with an exponent close to 6, consistent with density-scaling exponents for LJ systems determined in isomorph studies.[17] The systems studied by Assael *et al.* include alkanes,[87] simple organic molecules,[88] mixtures of *n*-alkanes,[89] *n*-alcohols,[92] refrigerants,[93] and more recently, ionic liquids.[95] In fact, their analysis is not just consistent with isomorph theory but shows the existence of isodynes–curves [in their formalism, curves along which the "reduced molar volume" $V_r \equiv V/V_0(T)$ is constant] along which three transport quantities are invariant in reduced units. This work constitutes a large body of experimental evidence for isodynes. The theoretical basis for their analysis is the hard-sphere model for which the transport coefficients are known and appropriate adjustment factors to account for the non-spherical nature of the molecules.

The important conclusion from the work of Dymond *et al.* is that the transport coefficients can be invariant on scaling with isomorph units without any reference to structural scaling (i.e., isomorph behavior) and, therefore, isodynes may be more prevalent than isomorphs, and it is perhaps isomorphs that are, in fact, the exception rather than the rule outside the domain of model systems, such as Lennard-Jones. In addition, recent papers by Khrapak and Khrapak[38,39] indicate that one can have isodynes without isomorphs in the context of reference density scaling, which is observed at low and medium densities (see also Ref. 40). The relatively recent investigations of viscuits (single trajectory contributions to the viscosity) also suggest that there is an underlying common invariance to the factors that determine the values of the transport coefficients that is insensitive to state point.[97–100]

The discovery of isodynes can be viewed as opening a way to generalize isomorph theory. Apart from isomorphs, a natural framework is Rosenfeld excess entropy scaling,[66] while another generalization of the isomorph concept for molecular systems introduced the term pseudo-isomorphs.[101] Rosenfeld's excess-entropy scaling has recently been reviewed by Dyre[45] and has typically concerned the three properties of viscosity, self-diffusion, and thermal conductivity, whose values in reduced units are fixed by the excess entropy,

$$S_{ex} \equiv S(\rho, T) - S_{id}(\rho, T), \tag{9}$$

where S is the full entropy and S_{id} is the entropy of the ideal gas at the same density and temperature. Excess-entropy scaling can be justified if a system can be mapped either to a hard-sphere system or to an inverse power law system, but neither of these seems plausible in the case of a complex molecular system such as the one studied here. There is no consensus as to the origin of excess-entropy scaling; clearly it follows when there are exact or approximate isomorphs, such that both structure and dynamics are invariant in reduced units along curves of constant excess entropy (configurational adiabats). However, liquids involving flexible molecules can have isomorphs that are not strictly configurational adiabats. The contribution to excess entropy from flexible bonds, for example, is decoupled from the invariant dynamics and structure. In some simple cases, isomorphs can be generated by removing the bond dynamics according to a preset procedure.[101] The resulting isomorphs are termed "pseudo-isomorphs" to emphasize that they are not configurational adiabats. Moreover, atomic systems with charge can exhibit invariant dynamics but not invariant structure on configurational adiabats.[36] In fact, considering the three types of invariant quantity, the following situations may be considered:

A. Invariant structure (full or partial).
B. Invariant dynamics (full or partial).
C. Correspondance of A or B with invariant excess entropy.

We can identify systems with all three characteristics (true isomorphs), just A and B (pseudoisomorphs), just B and C (simple ionic liquids, excess entropy scaling), or just B (complex ionic and small molecule liquids). In particular, isomorphs constitute a special case of isodynes, while excess entropy scaling and isodynes both constitute generalizations. The underlying connection between these related concepts is as yet unclear: Dyre concluded that "it remains an open question whether all aspects of excess-entropy scaling and related regularities reflect hidden scale invariance in one form or another."[45] This question remains open, and we believe that isodynes are part of the resolution of this issue. A theoretical framework is required to unify these different combinations. It is likely that coarse-graining, to be discussed in Sec. V B, has a key role to play.

B. Coarse-graining

Coarse-graining, the simplification of a model system by removing some of the degrees of freedom, is often presented as a practical tool to increase the time scales of simulations; a natural requirement is that the overall dynamics of the remaining degrees of freedom be preserved (apart from a possible rescaling of time; typically, the coarse grained system intrinsically evolves faster than the original[48]). However, it can also be a conceptual tool to understand how simplicity emerges in complex systems when irrelevant microscopic degrees of freedom are ignored. Ideally, one should be able to identify an analog to the excess entropy that is defined in the coarse-grained system and whose contours coincide with the isodynes. The fact that our two models, united-atom and all-atom, where the former can be understood as a coarse-graining of the latter, share isodynes is encouraging in this respect. In fact, we suggest that the preservation of isodynes, where they exist, should be a requirement of any reliable coarse-graining procedure.

Our results can be encapsulated by the statement that "coarse-grained dynamics are simple." The coarse-grained dynamics includes the dynamical quantities that are defined for a suitably coarse-grained model, such as shear-viscosity, self-diffusion, and most molecular rotations. In other words, these are *inter*molecular dynamics but not *intra*molecular dynamics (which is largely decoupled from isodynes). "Simple" means that isodynes exist, in effect making the phase diagram one-dimensional as far as dynamics is concerned. The molecular rotations that are not invariant on isodynes, i.e., are decoupled from isodynes, can be characterized as

those with lower moments of inertia, for example, a rotation about the long axis of TFSI, Fig. 16(b). However, it is not the moment of inertia itself that is relevant; it is more that such rotations disappear as degrees of freedom under sufficient coarse graining, under which, for example, TFSI would be represented as a cylinder with rounded ends.

Another example of the distinction between invariant CG degrees of freedom and decoupled intra-molecular degrees of freedom turns up in the stress autocorrelation function, whose overall decay is quite invariant along isodynes but in which the small wiggles, presumably associated with intra-molecular degrees of freedom, are not.

However, just as coarse-graining, as a simulation technique, does not in practice guarantee faithful reproduction of dynamics,[102,103] as a conceptual tool, it is not guaranteed that a simple entropy-like quantity characterizing isodynes can be identified. Moreover, coarse-graining would not seem to be able to explain the case of simple ionic liquids, which have isodynes but not isomorphs, since there are no obvious degrees of freedom that could be removed. Coarse-graining a complex ionic liquid would still leave the charge-ordering unaffected, an aspect of structure that is not invariant.

We consider that a carefully designed CG model could, in principle, illuminate the phenomenon of isodynes. It is significant that the AA version of our model seems to have essentially the same isodynes as the UA model. However, there is a question of how to guarantee this feature if one were to develop a more coarse-grained model than the UA one. One proposal in the literature, based on the concept of relative entropy, addresses more or less explicitly the slope of isodynes by coarse-graining to soft-sphere systems (inverse power-law potentials).[104] Ideally, one would not explicitly target the shapes of isodynes but identify some structural property whose consistency from AA to UA to CG would ensure the consistency of the isodynes; in that case, one could claim to have understood the presence of the latter in the more fine grained models. In fact, preserving the location of isodynes could be a useful criterion for confirming dynamical consistency between the AA and CG models.

VI. SUMMARY AND PERSPECTIVES

The main results of this work can be summarized as follows:

1. For these model ionic liquids, there exists a set of curves, termed isodynes, along which a number of dynamical quantities are invariant, even though there are no isomorphs for these systems.
2. The curves $T(\rho)$ along an isodyne can be well fitted by an exponential form, which corresponds to a density scaling exponent, γ, which increases with increasing density along a given isodyne. When considering the overall picture of how γ varies in the phase diagram, however, it depends more on temperature than on density [Fig. 8(b)].
3. The quantities that have been tested and shown to be (approximately) invariant are viscosity, the stress auto-correlation function, the mean squared displacement and the diffusion coefficient, and several rotational correlation functions. Of these, three are associated with cation rotations and one with anion rotation.
4. One tested anion rotational correlation function was not invariant. This is sensitive to rotations about the "long axis" of the molecule. A consequence of this lack of invariance is that this motion is not very important for, and is largely decoupled from, the general behavior of the liquid and could be "coarse-grained away."

We are far from having exhausted the possibilities for studying dynamical invariances in this IL system. With the exception of viscosity and the stress-autocorrelation function, our analyses pertained only to single-molecule dynamical properties. A natural next step would be to investigate the correlated motion of ions. One issue is the existence of ion pairs.[22] Correlations are particularly important in the context of the electrical conductivity, where they lead to departures from the Nernst–Einstein relation,[73,105] according to which the electrical conductivity is determined by the diffusivities of the ions without regard to correlations. Furthermore, it is plausible that correlations are strongly affected by Coulomb interactions and thus might be a dynamical feature that varies along isodynes, i.e., an exception to dynamical invariance.

Regarding the relation between isodynes and coarse-graining, the role of charges seems to be separate from that of intra-molecular degrees of freedom. Work on non-charged, but otherwise complex and flexible, molecular systems will also be necessary to better clarify this. To summarize, it is clear from this work that molecular simulation will continue to be an important tool in helping to understand and characterize these complex charged molecular systems, and in particular, the identification of isodynes, performed here for the first time, will be relevant for providing guidelines for designing practical applications involving them.

SUPPLEMENTAL MATERIAL

The supplementary material contains further details of the model and force field, including tables of parameters, a description of our approach to handling Coulomb forces, tests relating to cut-offs, details relating to the analysis, and additional data for rotational correlations.

ACKNOWLEDGMENTS

We acknowledge Dr. Lorenzo Costigliola (Roskilde University, Denmark) for helpful discussions. Funding from the Danish Ministry of Higher Education and Science through the ESS SMART Lighthouse is gratefully acknowledged. D.D. acknowledges the Royal Academy of Engineering for funding his Shell/RAEng Research Chair in Complex Engineering Interfaces and the EPSRC for the Prosperity Partnership No. EP/V038044/1. D.D. and D.M.H. acknowledge the support received from the EPSRC under the Established Career Fellowship Grant No. EP/N025954/1.

AUTHOR DECLARATIONS

Conflict of Interest

The authors have no conflicts to disclose.

Author Contributions

Peter A. Knudsen: Data curation (lead); Formal analysis (lead); Investigation (lead); Methodology (equal); Software (equal); Visualization (lead); Writing – original draft (equal). **David M. Heyes**: Supervision (supporting); Visualization (supporting); Writing – original draft (supporting); Writing – review & editing (equal). **Kristine Niss**: Conceptualization (lead); Funding acquisition (lead); Project administration (lead); Supervision (equal); Visualization (supporting); Writing – review & editing (supporting). **Daniele Dini**: Supervision (equal); Visualization (supporting); Writing – review & editing (supporting). **Nicholas P. Bailey**: Conceptualization (equal); Data curation (supporting); Formal analysis (supporting); Methodology (equal); Project administration (equal); Software (lead); Supervision (lead); Visualization (equal); Writing – original draft (lead); Writing – review & editing (equal).

DATA AVAILABILITY

Scripts and data files sufficient to generate the figures of the manuscript, as well as the Python scripts for running the simulations themselves, have been uploaded to Zenodo, https://doi.org/10.5281/zenodo.10451000.

REFERENCES

[1] A. Tölle, H. Schober, J. Wuttke, O. Randl, and F. Fujara, Phys. Rev. Lett. **80**, 2374 (1998).
[2] C. Alba-Simionesco, A. Cailliaux, A. Alegria, and G. Tarjus, Europhys. Lett. **68**, 58 (2004).
[3] R. Casalini and C. M. Roland, Phys. Rev. E **69**, 062501 (2004).
[4] *Transport Properties of Fluids: Their Correlation, Prediction and Estimation*, edited by J. Millat, J. H. Dymond, and C. A. Nieto de Castro (Cambridge University Press, 1996), ISBN: 978-0-521-46178-8.
[5] C. M. Roland, S. Hensel-Bielowka, M. Paluch, and R. Casalini, Rep. Prog. Phys. **68**, 1405 (2005).
[6] K. Niss and T. Hecksher, J. Chem. Phys. **149**, 230901 (2018).
[7] K. L. Ngai, R. Casalini, S. Capaccioli, M. Paluch, and C. M. Roland, J. Phys. Chem. B **109**, 17356 (2005).
[8] K. Adrjanowicz, J. Pionteck, and M. Paluch, RSC Adv. **6**, 49370 (2016).
[9] K. Ngai and M. Paluch, J. Non-Cryst. Solids **478**, 1 (2017).
[10] H. W. Hansen, A. Sanz, K. Adrjanowicz, B. Frick, and K. Niss, Nat. Commun. **9**, 518 (2018).
[11] H. W. Hansen, B. Frick, S. Capaccioli, A. Sanz, and K. Niss, J. Chem. Phys. **149**, 214503 (2018).
[12] N. Gnan, T. B. Schrøder, U. R. Pedersen, N. P. Bailey, and J. C. Dyre, J. Chem. Phys. **131**, 234504 (2009).
[13] T. B. Schrøder and J. C. Dyre, J. Chem. Phys. **141**, 204502 (2014).
[14] J. C. Dyre, J. Phys. Chem. B **118**, 10007 (2014).
[15] C. M. Roland, Macromolecules **43**, 7875 (2010).
[16] F. Hummel, G. Kresse, J. C. Dyre, and U. R. Pedersen, Phys. Rev. B **92**, 174116 (2015).
[17] N. P. Bailey, U. R. Pedersen, N. Gnan, T. B. Schrøder, and J. C. Dyre, J. Chem. Phys. **129**, 184507 (2008).
[18] T. B. Schrøder, N. P. Bailey, U. R. Pedersen, N. Gnan, and J. C. Dyre, J. Chem. Phys. **131**, 234503 (2009).
[19] S. Pawlus, M. Paluch, J. Ziolo, and C. M. Roland, J. Phys.: Condens. Matter **21**, 332101 (2009).
[20] L. A. Roed, D. Gundermann, J. C. Dyre, and K. Niss, J. Chem. Phys. **139**, 101101 (2013).
[21] M. Romanini, M. Barrio, R. Macovez, M. D. Ruiz-Martin, S. Capaccioli, and J. L. Tamarit, Sci. Rep. **7**, 1346 (2017).
[22] Y.-L. Wang, B. Li, S. Sarman, F. Mocci, Z.-Y. Lu, J. Yuan, A. Laaksonen, and M. D. Fayer, Chem. Rev. **120**, 5798 (2020).
[23] C. M. Roland, S. Bair, and R. Casalini, J. Chem. Phys. **125**, 124508 (2006).
[24] A. S. Pensado, A. A. H. Pádua, M. J. P. Comuñas, and J. Fernández, J. Phys. Chem. B **112**, 5563 (2008).
[25] M. Paluch, S. Haracz, A. Grzybowski, M. Mierzwa, J. Pionteck, A. Rivera-Calzada, and C. Leon, J. Phys. Chem. Lett. **1**, 987 (2010).
[26] E. R. López, A. S. Pensado, M. J. Comuñas, A. A. Pádua, J. Fernández, and K. R. Harris, J. Chem. Phys. **134**, 144507 (2011).
[27] M. Paluch, E. Masiewicz, A. Grzybowski, S. Pawlus, J. Pionteck, and Z. Wojnarowska, J. Chem. Phys. **141**, 134507 (2014).
[28] Z. Wojnarowska, G. Jarosz, A. Grzybowski, J. Pionteck, J. Jacquemin, and M. Paluch, Phys. Chem. Chem. Phys. **16**, 20444 (2014).
[29] K. R. Harris and M. Kanakubo, Phys. Chem. Chem. Phys. **17**, 23977 (2015).
[30] M. Paluch, Z. Wojnarowska, P. Goodrich, J. Jacquemin, J. Pionteck, and S. Hensel-Bielowka, Soft Matter **11**, 6520 (2015).
[31] Z. Wojnarowska, L. Tajber, and M. Paluch, J. Phys. Chem. B **123**, 1156 (2019).
[32] K. R. Harris and M. Kanakubo, Phys. Chem. Chem. Phys. **24**, 14430 (2022).
[33] K. R. Harris, M. Kanakubo, D. Kodama, T. Makino, Y. Mizuguchi, Y. Suzuki, and T. Watanabe, J. Chem. Eng. Data **68**, 549 (2023).
[34] H. W. Hansen, F. Lundin, K. Adrjanowicz, B. Frick, A. Matic, and K. Niss, Phys. Chem. Chem. Phys. **22**, 14169 (2020).
[35] P. A. Knudsen, Ph.D. thesis, Roskilde University, 2022.
[36] P. A. Knudsen, K. Niss, and N. P. Bailey, J. Chem. Phys. **155**, 054506 (2021).
[37] I. H. Bell, R. Fingerhut, J. Vrabec, and L. Costigliola, J. Chem. Phys. **157**, 074501 (2022).
[38] S. A. Khrapak and A. G. Khrapak, Phys. Rev. E **103**, 042122 (2021).
[39] S. A. Khrapak and A. G. Khrapak, J. Phys. Chem. Lett. **13**, 2674 (2022).
[40] D. M. Heyes, D. Dini, S. Pieprzyk, and A. C. Brańka, J. Chem. Phys. **158**, 134502 (2023).
[41] T. B. Schrøder, U. R. Pedersen, N. P. Bailey, S. Toxvaerd, and J. C. Dyre, Phys. Rev. E **80**, 041502 (2009).
[42] L. V. Woodcock, Proc. R. Soc. London, Ser. A **348**, 187 (1976).
[43] J. M. Young, I. H. Bell, and A. H. Harvey, J. Chem. Phys. **158**, 024502 (2023).
[44] R. Macías-Salinas and J. Gross, Fluid Phase Equilib. **574**, 113897 (2023).
[45] J. C. Dyre, J. Chem. Phys. **149**, 210901 (2018).
[46] A. Saliou, P. Jarry, and N. Jakse, Phys. Rev. E **104**, 044128 (2021).
[47] J. Jin, K. S. Schweizer, and G. A. Voth, J. Chem. Phys. **158**(3), 034103 (2023).
[48] J. P. Ewen, C. Gattinoni, F. M. Thakkar, N. Morgan, H. A. Spikes, and D. Dini, Materials **9**, 651 (2016).
[49] W. L. Jorgensen, J. Chandrasekhar, J. D. Madura, R. W. Impey, and M. L. Klein, J. Chem. Phys. **79**, 926 (1983).
[50] W. L. Jorgensen and J. Tirado-Rives, J. Am. Chem. Soc. **110**, 1657 (1988).
[51] W. L. Jorgensen, D. S. Maxwell, and J. Tirado-Rives, J. Am. Chem. Soc. **118**, 11225 (1996).
[52] S. V. Sambasivarao and O. Acevedo, J. Chem. Theory Comput. **5**, 1038 (2009).
[53] B. Doherty, X. Zhong, S. Gathiaka, B. Li, and O. Acevedo, J. Chem. Theory Comput. **13**, 6131 (2017).
[54] J. N. Canongia Lopes and A. A. H. Pádua, J. Phys. Chem. B **108**, 16893 (2004).
[55] H. Xing, X. Zhao, Q. Yang, B. Su, Z. Bao, Y. Yang, and Q. Ren, Ind. Eng. Chem. Res. **52**, 9308 (2013).
[56] W. D. Cornell, P. Cieplak, C. I. Bayly, I. R. Gould, K. M. Merz, D. M. Ferguson, D. C. Spellmeyer, T. Fox, J. W. Caldwell, and P. A. Kollman, J. Am. Chem. Soc. **118**, 2309 (1996).
[57] Z. Liu, S. Huang, and W. Wang, J. Phys. Chem. B **108**, 12978 (2004).
[58] W. L. Jorgensen, J. D. Madura, and C. J. Swenson, J. Am. Chem. Soc. **106**, 6638 (1984).
[59] A. M. Smondyrev and M. L. Berkowitz, J. Comput. Chem. **20**, 531 (1999).
[60] A. K. Giri and E. Spohr, J. Mol. Liq. **228**, 63 (2017).
[61] N. Bailey, T. Ingebrigtsen, J. S. Hansen, A. Veldhorst, L. Bøhling, C. Lemarchand, A. Olsen, A. Bacher, L. Costigliola, U. Pedersen *et al.*, SciPost Phys. **3**, 038 (2017).
[62] C. Xu and Z. Cheng, Processes **9**, 337 (2021).

[63]J. O. Valderrama, L. A. Forero, and R. E. Rojas, Ind. Eng. Chem. Res. **51**, 7838 (2012).
[64]K. R. Harris, L. A. Woolf, M. Kanakubo, and T. Rüther, J. Chem. Eng. Data **56**, 4672 (2011).
[65]J. P. Hansen and I. R. McDonald, Phys. Rev. A **11**, 2111 (1975).
[66]Y. Rosenfeld, Phys. Rev. A **15**, 2545 (1977).
[67]J. H. Dymond, Int. J. Thermophys. **18**, 303 (1997).
[68]Note 1, the contourfunction in the Matplotlib Python library.
[69]A. Z. Panagiotopoulos, J. Phys.: Condens. Matter **17**, S3205 (2005).
[70]U. Balucani and M. Zoppi, *Dynamics of the Liquid State* (Clarendon Press, Oxford, 1994), ISBN: 9780198517399.
[71]T. Köddermann, R. Ludwig, and D. Paschek, ChemPhysChem **9**, 1851 (2008).
[72]M. Kanakubo, K. R. Harris, N. Tsuchihashi, K. Ibuki, and M. Ueno, J. Phys. Chem. B **111**, 2062 (2007).
[73]H. Liu and E. Maginn, J. Chem. Phys. **135**, 124507 (2011).
[74]J. C. Araque, S. K. Yadav, M. Shadeck, M. Maroncelli, and C. J. Margulis, J. Phys. Chem. B **119**, 7015 (2015).
[75]L. Costigliola, D. M. Heyes, T. B. Schrøder, and J. C. Dyre, J. Chem. Phys. **150**, 021101 (2019).
[76]R. Zwanzig, J. Chem. Phys. **79**, 4507 (1983).
[77]R. Zwanzig and A. K. Harrison, J. Chem. Phys. **83**, 5861 (1985).
[78]N. H. March and M. P. Tosi, Phys. Rev. E **60**, 2402 (1999).
[79]N. H. March and J. A. Alonso, Phys. Rev. E **73**, 032201 (2006).
[80]J. C. M. Li and P. Chang, J. Chem. Phys. **23**, 518 (1955).
[81]R. E. Meyer and N. H. Nachtrieb, J. Chem. Phys. **23**, 1851 (1955).
[82]S. Khrapak and A. Khrapak, Phys. Rev. E **104**, 044110 (2021).
[83]S. Khrapak and A. Khrapak, J. Chem. Phys. **158**, 206101 (2023).
[84]U. Bengtzelius, W. Götze, and A. Sjölander, J. Phys. C: Solid State Phys. **17**, 5915 (1984).
[85]W. Götze and L. Sjögren, Rep. Prog. Phys. **55**, 241 (1992).
[86]O. Borodin and G. D. Smith, J. Phys. Chem. B **110**, 11481 (2006).
[87]M. J. Assael, J. H. Dymond, M. Papadaki, and P. M. Patterson, Int. J. Thermophys. **13**, 269 (1992).
[88]M. J. Assael, J. H. Dymond, M. Papadaki, and P. M. Patterson, Fluid Phase Equilib. **75**, 245 (1992).
[89]M. J. Assael, J. H. Dymond, M. Papadaki, and P. M. Patterson, Int. J. Thermophys. **13**, 659 (1992).
[90]M. J. Assael, J. H. Dymond, and P. M. Patterson, Int. J. Thermophys. **13**, 729 (1992).
[91]M. J. Assael, J. H. Dymond, and P. M. Patterson, Int. J. Thermophys. **13**, 895 (1992).
[92]M. J. Assael, J. H. Dymond, and S. K. Polimatidou, Int. J. Thermophys. **15**, 189 (1994).
[93]M. J. Assael, J. H. Dymond, and S. K. Polimatidou, Int. J. Thermophys. **16**, 761 (1995).
[94]M. J. Assael, A. E. Kalyva, K. E. Kakosimos, and K. D. Antoniadis, Int. J. Thermophys. **30**, 1733 (2009).
[95]F. M. Gaciño, M. J. P. Comuñas, J. Fernández, S. K. Mylona, and M. J. Assael, Int. J. Thermophys. **35**, 812 (2014).
[96]L. Costigliola, U. R. Pedersen, D. M. Heyes, T. B. Schrøder, and J. C. Dyre, J. Chem. Phys. **148**, 081101 (2018).
[97]D. M. Heyes, E. R. Smith, and D. Dini, J. Chem. Phys. **150**, 174504 (2019).
[98]D. M. Heyes, D. Dini, and E. R. Smith, J. Chem. Phys. **152**, 194504 (2020).
[99]D. M. Heyes, D. Dini, and E. R. Smith, J. Chem. Phys. **154**, 074503 (2021).
[100]D. M. Heyes and D. Dini, J. Chem. Phys. **156**, 124501 (2022).
[101]A. E. Olsen, J. C. Dyre, and T. B. Schrøder, J. Chem. Phys. **145**, 241103 (2016).
[102]S. Kloth, M. P. Bernhardt, N. F. A. van der Vegt, and M. Vogel, J. Phys.: Condens. Matter **33**, 204002 (2021).
[103]J. F. Rudzinski, S. Kloth, S. Wörner, T. Pal, K. Kremer, T. Bereau, and M. Vogel, J. Phys.: Condens. Matter **33**, 224001 (2021).
[104]M. S. Shell, J. Chem. Phys. **137**, 084503 (2012).
[105]A. Afandak and H. Eslami, J. Phys. Chem. B **121**, 7699 (2017).